Microscopic description of the $\alpha+^{16}O$ system in a multicluster model

M. Dufour,* P. Descouvemont, and D. Baye
Physique Nucléaire Théorique et Physique Mathématique, C.P. 229, Université Libre de Bruxelles, Campus Plaine, B1050 Bruxelles, Belgium
(Received 8 March 1994)

The multicluster generator coordinate method is applied to a microscopic study of the ^{20}Ne spectroscopy and of the $^{16}O(\alpha,\gamma)^{20}Ne$ capture cross section. The ^{16}O nucleus is described by four α clusters located on the apexes of a tetrahedron. The good quantum numbers of the ^{16}O and $\alpha+^{16}O$ wave functions are restored by a multiple angular-momentum projection. With respect to the usual two-center approach, where ^{16}O is described by a closed p shell, the five-α model improves different ^{20}Ne spectroscopic properties. The $^{16}O(\alpha,\gamma)^{20}Ne$ S factor is reduced by about 30% at astrophysical energies.

PACS number(s): 21.60.Gx, 25.55.Ci, 27.30.+t

I. INTRODUCTION

The microscopic α model, introduced many years ago [1], has been applied to several $4N$ systems (see a review in Ref. [2]). Owing to its large binding energy, the α particle plays an important role in the structure of these systems. In addition to the simple ^{8}Be nucleus, a fairly good description of ^{12}C and ^{16}O nuclei can be obtained in the α model. This model has also been applied to ^{20}Ne and ^{24}Mg, and predicts highly excited states, presenting a linear α-chain structure [3].

The application of the α model to reactions is more recent. If more than two α clusters are involved in the system, a correct treatment of boundary conditions requires the restoration of good quantum numbers in each colliding nuclei. In this case, angular momentum projection must be performed not only on the total spin of the system, but also on the individual spins of the nuclei. In 1987, we used the generator-coordinate method (GCM) to investigate the $^{8}Be(\alpha,\gamma)^{12}C$ capture reaction in a three-α model [4]. In that study, the ^{8}Be nucleus is described by a quasibound $\alpha+\alpha$ structure, which provides a realistic description of the ground and first excited states. The microscopic 12-nucleon wave functions are antisymmetrized, and projected on the ^{8}Be and ^{12}C good quantum numbers. We have shown that, in the three-cluster approach, GCM matrix elements between projected wave functions are obtained from five-dimensional integrals of nonprojected matrix elements [4]. If the calculation of these nonprojected matrix elements is fairly simple in the α model, the projection on good quantum numbers leads to large computer times.

The α model has been then extended to the $\alpha+^{12}C$ system [5], where the ^{12}C nucleus is described by three α particles located on the apexes of an equilateral triangle. It is shown in Ref. [5] that the $\alpha+^{12}C$ phase shifts and the $^{12}C(\alpha,\gamma)^{16}O$ capture cross section are sensitive to clustering effects in ^{12}C. In that system, the calculation of GCM matrix elements involves seven-dimensional integrals. However, the occurrence of only α particles allows an efficient vectorization of the codes, and makes that calculation feasible.

In the present paper, we aim at investigating the $\alpha+^{16}O$ system in a five-α model. The ^{16}O wave functions are described by four α particles in a tetrahedral structure. Our goal for the future is to extend this five-cluster approach to systems involving three α particles and two $0s$ clusters, such as $^{13}N+p$ or $^{15}O+\alpha$ for example. In a one-center description of ^{16}O, the $\alpha+^{16}O$ system has been investigated by several authors [2,6]. This two-center model will be used here as a starting point for a comparison between different microscopic approaches. The advantages of the α multicluster model are an improvement of the ^{16}O ground-state energy with respect to the one-center description (i.e., a better account of saturation), and a straightforward inclusion of some $\alpha+^{16}O^{*}$ excited channels.

The $^{16}O(\alpha,\gamma)^{20}Ne$ capture cross section is expected to be negligible for helium burning in stars [7]. However, this reaction is one of the best tests for microscopic models, since realistic wave functions of ^{16}O and α are available. It is therefore a suitable case for comparing different approaches.

In Secs. II and III, we briefly present the model, and the conditions of the calculation. Section IV is devoted to the ^{20}Ne spectroscopy; $\alpha+^{16}O$ elastic phase shifts and $^{16}O(\alpha,\gamma)^{20}Ne$ cross sections are presented in Sec. V. Concluding remarks and possible extensions are discussed in Sec. VI.

II. THE MICROSCOPIC α MODEL

Details on microscopic models and on the GCM can be found in Refs. [8–10] for example. Here, we restrict ourselves to the peculiarities of the five-α description of

*Permanent address: Centre de Recherches Nucléaires, 23 rue du Loess, F67037 Strasbourg, France.

the α+^{16}O system. Let Φ_α (**S**) be a Slater determinant for the α particle, involving $0s$ harmonic oscillator wave functions with parameter b, and centered at **S**. We then consider four α particles located at $\mathbf{S}_1$, $\mathbf{S}_2$, $\mathbf{S}_3$, and $\mathbf{S}_4$, where $\mathbf{S}_i$ represents the ith apex of a tetrahedron (see Fig. 1). The basis of this tetrahedron, which corresponds to a ^{12}C nucleus, is assumed to be equilateral with a side R_C; the height is denoted as R_h.

An ^{16}O wave function $\phi^{I\nu\pi}_{O,K}$ with spin I, parity π, projection ν, and intrinsic projection K (the z axis of the intrinsic ^{16}O frame is along the height of the tetrahedron) reads

$$\phi^{I\nu\pi}_{O,K}(R_C,R_h)=\phi^{-1}_{\text{c.m.}}\,\frac{1}{2}(1+\pi P)\int d\Omega\; D^{I\star}_{\nu K}(\Omega)\;\mathcal{R}(\Omega)\;\mathcal{A}\;\Phi_\alpha(\mathbf{S}_1)\Phi_\alpha(\mathbf{S}_2)\Phi_\alpha(\mathbf{S}_3)\Phi_\alpha(\mathbf{S}_4), \tag{1}$$

where the $\mathbf{S}_i$ depend on R_C and R_h, and $\phi_{\text{c.m.}}$ is a center-of-mass (c.m.) Gaussian function. In (1), Ω represents the Euler angles, $D^I_{\nu K}(\Omega)$ is a Wigner function, and $\mathcal{R}(\Omega)$ and P are the rotation and parity operators with respect to the tetrahedron c.m. Some remarkable properties arise from the equilateral triangle assumption. (i) The symmetry reduces the integration domain by a factor of 3, and makes the parity projection very simple. (ii) The number of K values is limited by the relationship $K=3n$, where n is a positive integer number. (iii) If the tetrahedron is symmetric ($R_h=\sqrt{2/3}R_C$), I values different from $I=3n$ are forbidden.

Let us now turn to the ^{20}Ne wave functions, and consider a further α particle located at a distance **R** from the ^{16}O c.m. A five-α Slater determinant can be written as (see Fig. 1)

$$\begin{aligned}\Phi_{5\alpha}(\mathbf{R},R_C,R_h,\Omega)=\mathcal{A}\;&\Phi_\alpha[-\tfrac{1}{5}\mathbf{R}+\mathbf{S}_1(\Omega)]\;\Phi_\alpha[-\tfrac{1}{5}\mathbf{R}+\mathbf{S}_2(\Omega)]\\ &\times\Phi_\alpha[-\tfrac{1}{5}\mathbf{R}+\mathbf{S}_3(\Omega)]\;\Phi_\alpha[-\tfrac{1}{5}\mathbf{R}+\mathbf{S}_4(\Omega)]\;\Phi_\alpha(\tfrac{4}{5}\mathbf{R}),\end{aligned} \tag{2}$$

where $\mathbf{S}_i(\Omega)$ represents the vector $\mathbf{S}_i$ after the rotation Ω. This intrinsic wave function must be projected on the ^{16}O spin I, and then on the total angular momentum J and parity π of the 20-nucleon system. One obtains, using (1) and (2):

$$\begin{aligned}\Phi^{JM\pi}_{\ell I,K}(R,R_C,R_h)=\frac{1}{2}\sum_\nu\langle\ell I\;M-\nu\;\nu\;|JM\rangle\int d\hat{\mathbf{R}}\;d\Omega\;Y^{M-\nu}_\ell(\hat{\mathbf{R}})\;[D^I_{\nu K}\;(\Omega)\\ +\pi(-)^{I+K}D^I_{\nu-K}\;(\Omega)]\;\Phi_{5\alpha}(\mathbf{R},R_C,R_h,\Omega),\end{aligned} \tag{3}$$

where ℓ is the relative orbital momentum between α and ^{16}O. These basis functions will be used for ^{20}Ne bound states or resonances, as well as for α+^{16}O scattering states. The total wave functions $\Psi^{JM\pi}$ are given by

$$\Psi^{JM\pi}=\sum_{\ell IK}\int dR\;dR_C\;dR_h\;f^{J\pi}_{\ell I,K}(R,R_C,R_h)\;\Phi^{JM\pi}_{\ell I,K}(R,R_C,R_h) \tag{4}$$

where the generator functions $f^{J\pi}_{\ell I,K}$ are determined in the microscopic R-matrix method (MRM) (see Refs. [11,12]). In practice, Eq. (4) is discretized over a finite set of (R,R_C,R_h) values, and the generator functions are derived from matrix elements of the 20-body Hamiltonian between basis functions (3). Using (2) and (3), the reduced matrix element of an irreducible tensor operator O_λ reads

$$\begin{aligned}\langle\Phi^{J\pi}_{\ell I,K}(R,R_C,R_h)\;||O_\lambda||\;\Phi^{J'\pi'}_{\ell'I',K'}(R',R'_C,R'_h)\rangle=2\pi^2\sum_{\nu\nu'\mu}&\langle J'\lambda\nu-\mu\mu|J\nu\rangle\langle\ell I0\nu|J\nu\rangle\langle\ell'I'\nu-\nu'-\mu\;\nu'|J'\nu-\mu\rangle\\ \times\int Y^0_\ell(0,0)\;[D^{I\star}_{\nu K}(\Omega)\;&+\;\pi(-)^{I+K}D^{I\star}_{\nu-K}(\Omega)]\;Y^{\nu-\nu'-\mu}_{\ell'}(\theta,0)\\ \times[D^{I'}_{\nu'K'}(\Omega')&+\pi'(-)^{I'+K'}D^{I'}_{\nu'-K'}(\Omega')]\\ \times\langle\Phi_{5\alpha}(\mathbf{R},R_C,R_h,\Omega)\;|O_{\lambda\mu}|\;&\Phi_{5\alpha}(\mathbf{R}',R'_C,R'_h,\Omega'))d\cos\theta\;d\Omega\;d\Omega',\end{aligned} \tag{5}$$

where **R** is along the z axis, and $\mathbf{R}'$ makes an angle θ with respect to **R**, and is located in the x-z plane. This calculation is similar to that of the α+^{12}C system [5]. The main characteristic of GCM matrix elements is to involve seven-dimensional integrals which, for reaching a good accuracy, need very long computer times. Our efforts were therefore concentrated on the optimization of the matrix elements of the nucleon-nucleon interaction between Slater determinants (2). These matrix elements involve quadruple sums which can be efficiently vectorized when the number of centers is larger than three. A significant reduction of computer times arises from the

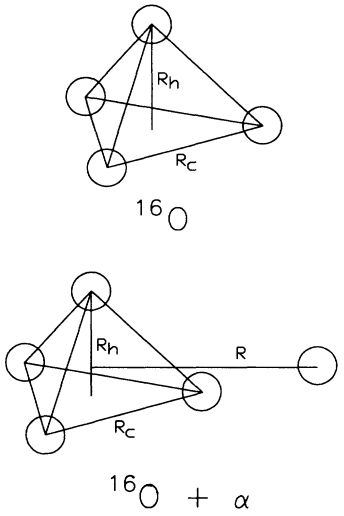

FIG. 1. Cluster structure of ^{16}O and ^{20}Ne, and definitions of the generator coordinates R_C, R_h, and R. α particles are represented by circles.

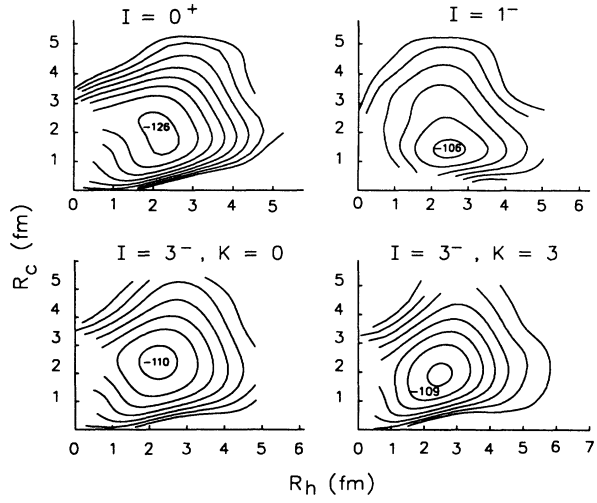

FIG. 2. Energy surfaces of different ^{16}O states, characterized by I, π, and K [see Eq. (6)]. The contour lines are plotted in steps of 2.5 MeV.

equilateral-triangle assumption for the tetrahedron basis. This symmetry reduces the integration domain in (5) by a factor of 9.

III. FOUR-α DESCRIPTION OF ^{16}O

Our previous investigation of the $\alpha+^{16}$O system [6] will be used as a starting point for a comparison between different microscopic approaches. We therefore employ the same nucleon-nucleon interaction $V2$ [13]; in the α model also, the spin-orbit and tensor components exactly vanish. The oscillator parameter is chosen as $b = 1.36$ fm, which minimizes the α binding energy with the V2 force.

In Fig. 2, we present the ^{16}O binding energies as a function of R_C and R_h. For given spin I, parity π and intrinsic projection K, it is defined as

$$E^{I\pi}_K(R_C,R_h) = \frac{\langle \Phi^{I\nu\pi}_{O,K}(R_C,R_h)\ |H|\ \Phi^{I\nu\pi}_{O,K}(R_C,R_h)\rangle}{\langle \Phi^{I\nu\pi}_{O,K}(R_C,R_h)\ |\ \Phi^{I\nu\pi}_{O,K}(R_C,R_h)\rangle}, \tag{6}$$

where H is the 16-nucleon Hamiltonian, and $\Phi^{I\nu\pi}_{O,K}(R_C,R_h)$ is given by (1). The Majorana parameter is taken as $M = 0.6326$; this choice will be explained in Sec. IV. The ^{16}O ground-state energy is found at $R_C = 1.88$ fm, and $R_h = 2.22$ fm, yielding $E^0_0 = -127.3$ MeV. This structure is rather far from a symmetric tetrahedron, where $R_h = \sqrt{2/3}R_C$. With the symmetric configuration, i.e., with a single degree of freedom in the ^{16}O description, the minimum energy is found for $R_C = 2.39$ fm, giving $E^0_0 = -127.0$ MeV. The small energy difference between both geometries indicates that a symmetric configuration would provide a fair description of the ground state. Since the use of any R_h value does not need additional computer times, we have kept this degree of freedom. However, as stated in Sec. II, removing the equilateral-triangle assumption for the tetrahedron basis would strongly increase computer times. The R_C value is smaller than for the ^{12}C nucleus ($R_C \simeq 2.8$ fm; see Ref. [5]), which means that the fourth α particle brings the other three α particles closer to each other. At the minimum, the rms radius of ^{16}O in the four-α model with pointlike nucleons is $\sqrt{\langle r^2\rangle} = 2.25$ fm, which is smaller than the experimental value $\sqrt{\langle r^2\rangle} = 2.59 \pm 0.02$ fm, deduced from the charge radius [14]. It is interesting to compare the binding energy and the radius with the corresponding values obtained in the one-center shell model, where ^{16}O is described by a filled p shell. With the same $V2$ force, the minimum is found at -116.8 MeV for an oscillator parameter b =1.55 fm and the rms radius is 2.28 fm. If the rms radii are similar, the improvement of the ^{16}O binding energy in the four-α model is better than 10 MeV.

This model also gives rise to excited states. The minima of the binding energies are obtained at $(R_C, R_h) =$ (1.40 fm, 2.46 fm) for $I = 1^-$, (2.41 fm, 2.24 fm) for $I = 3^-$, K=0, and (1.91 fm, 2.46 fm) for $I = 3^-$, K=3. An approximation of the 2^+_1 state can be found, but this state is well known to have a marked $\alpha+^{12}$C structure and therefore its description in the four-α model is very poor. Figure 2 shows that the 1^- and 3^- excitation energies are much larger than the experimental values (7.12 MeV and 6.03 MeV, respectively). This result is partly explained by the lack of spin-orbit effects in the α model, where the intrinsic spin S is zero.

IV. THE ^{20}NE SPECTROSCOPY

A. Conditions of the calculation

For computer-time reasons, the ^{16}O description is restricted to a single set of (R_C, R_h) values, which we

choose as $R_C = 1.8$ fm and $R_h = 2.5$ fm for the $\alpha+^{16}$O wave functions (3). These generator coordinates represent a compromise between the values obtained for the minima in the $I = 0^+$, 1^- and 3^- ^{16}O states, which are included in the GCM basis. For $I = 3^-$, the $K = 3$ component is small and requires methods of higher-accuracy for the numerical calculation of matrix elements; it has not been taken into account in (3). The ^{16}O energies are -126.6 MeV, -99.6 MeV, and -110.5 MeV for the 0^+, 1^-, and 3^- states, respectively. It is obvious that the too-high ^{16}O(1^-) and ^{16}O(3^-) energies do not allow a realistic investigation of $\alpha+^{16}$O scattering near the inelastic thresholds. However, as long as we are interested in low energies, such as astrophysical energies, the $\alpha+^{16}$O* channels are closed, and their role is restricted to distortion effects in the wave functions. At those energies, the threshold problem is less important, but an enlargement of the GCM basis improves the wave functions.

For the $\alpha+^{16}$O relative motion, the generator coordinates R (see Fig. 1) are chosen from 2.2 fm to 8.6 fm with a step of 0.8 fm. The bound-state, resonance, and scattering wave functions are calculated in the microscopic R-matrix method, described in Refs. [11,12].

In this paper, we mainly aim at investigating different microscopic approaches of the $\alpha+^{16}$O system. Our starting point is the two-center $\alpha+^{16}$O description [6] which will be compared to the single-channel five-α description, involving the $\alpha+^{16}$O(0^+) configuration only; this comparison will provide an estimate of clustering effects. It will be further extended to a multichannel study involving the $\alpha+^{16}$O(0^+, 3^-, 1^-) configurations. This step will illustrate the importance of the distortion due to excited channels in the ^{20}Ne spectroscopy, and in the $\alpha+^{16}$O scattering. If we use the standard Majorana parameter M=0.6, we find for the ground-state absolute energy -169.2, -184.8, and -187.1 MeV in the three models respectively. In the following, in order to make the comparison as meaningful as possible, the Majorana parameter has been fitted with the experimental ^{20}Ne(2^+) binding energy for each calculation (M = 0.6245, 0.6275, and 0.6326). This state plays a dominant role in the ^{16}O$(\alpha,\gamma)^{20}$Ne capture reaction.

B. The 0_1^+ and 0^- bands

Energy spectra of the $K = 0_1^+$ and $K = 0^-$ bands of ^{20}Ne are displayed in Fig. 3. The rotational constant

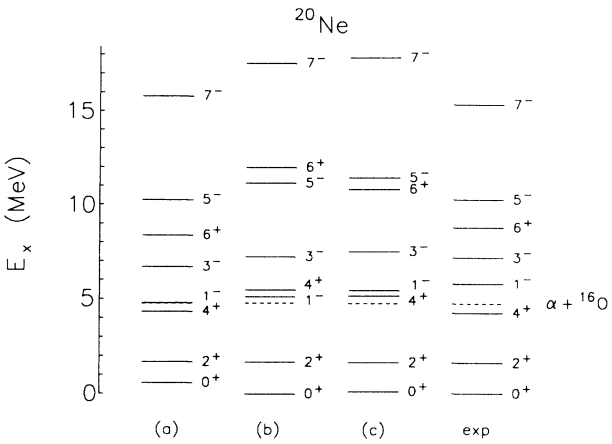

FIG. 3. Energy spectra of ^{20}Ne in the three models. The $\alpha+^{16}$O thresholds are represented by dashed lines. (a); two-center and (b), five-center $\alpha+^{16}$O(0^+); (c), five-center $\alpha+^{16}$O($0^+, 3^-, 1^-$).

of the 0_1^+ band is increased in the five-α model. This yields a very good $2^+ - 0^+$ energy difference, but reduces the energies of the higher band members. In negative parity, the band head of the 0^- band gets closer to the experimental value.

Spectroscopic properties of ^{20}Ne are gathered in Table I. Notice that the α width of a low-energy resonance is very sensitive to its location; accordingly, the values given in Table I have been obtained after a slight readjustment of the Majorana parameter for each state. Table I shows that α widths, which are significantly overestimated in the two-center approach, are all improved when clustering effects are included in ^{16}O. For the 6^+ resonance, the importance of $\alpha+^{16}$O* channels is higher than for members of the 0^- band. The slightly larger 0^+ rms radius and 2^+ quadrupole moment obtained in the two-center model partly arise from the larger oscillator parameter used in that description (b = 1.62 fm). The microscopic results remain too small with respect to experiment. This problem might be due to missing components in the nucleon-nucleon force, such as spin-orbit or three-body terms.

In Table II, we show reduced $E2$ transition probabilities in the different models. For the $2^+ \rightarrow 0^+$ and $4^+ \rightarrow 2^+$ transitions, the $B(E2)$ values are weakly sensitive to the ^{20}Ne description. In agreement with the 0^+ rms radius and 2^+ quadrupole moment (see Table I), the $2^+ \rightarrow$

TABLE I. Spectroscopic properties of ^{20}Ne. Energies are expressed in keV and lengths in fm.

J^π	Two centers	Five centers (0^+)	Five centers ($0^+, 3^-, 1^-$)	Expt. [15]
$\Gamma(6^+)$	0.53	0.50	0.30	0.11 ± 0.02
$\Gamma(1^-)$	0.042	0.032	0.031	0.028 ± 0.003
$\Gamma(3^-)$	13.0	10.8	10.6	8.2 ± 0.3
$\Gamma(5^-)$	200	173	169	145 ± 40
$\Gamma(7^-)$	700	570	530	310 ± 30
$\sqrt{\langle r^2 \rangle}(0^+)$	2.76	2.66	2.65	2.91[a]
$Q(2^+)$	−14.3	−14.1	−14.3	−27 ± 3

[a]From the charge radius [16].

TABLE II. $E2$ transition probabilities (in $e^2\text{fm}^4$) in ^{20}Ne.

$J_i^{\pi_i} \rightarrow J_f^{\pi_f}$	Two centers	Five centers (0^+)	Five centers ($0^+, 3^-, 1^-$)	Expt. [15]
$2^+ \rightarrow 0^+$	49.3	49.6	50.0	68 ± 4
$4^+ \rightarrow 2^+$	64.4	63.0	64.4	71 ± 7
$6^+ \rightarrow 4^+$	56.0	68.7	55.3	65 ± 10
$3^- \rightarrow 1^-$	178	157	155	164 ± 26
$5^- \rightarrow 3^-$	208	178	206	

0^+ transition probability is too small in the GCM. This result suggests that the deformation in ^{20}Ne low-lying states should be stronger.

C. Additional bands

The five-α model gives rise to high-energy narrow resonances, known as "Pauli resonances" or "almost forbidden states" [9,17]. These resonances are model dependent, and are characteristic of microscopic calculations where the colliding nuclei are not described by the same set of orbitals. This situation is met in two-cluster calculations with different oscillator parameters [18], or in multicluster calculations where one of the colliding nuclei itself is described by a cluster structure [5]. The number of Pauli resonances is equal to the number of forbidden states in two-cluster models with identical oscillator parameters. Their physical meaning is usually not simple. They are poor approximations of states which have a more complicated cluster structure than those included in the model (see Ref. [18]). Here, we do not aim to investigate these resonances in detail since they appear above 10 MeV, where many inelastic and reaction channels should be introduced for a realistic description of $\alpha+^{16}$O scattering. For example, the lowest Pauli resonance in the 0^+ partial wave is located at $E_{\text{c.m.}} = 14.3$ MeV with a width of 5.9 keV.

When the $\alpha+^{16}\text{O}(3^-)$ channel is taken into account, the model provides a band which can be assigned to the experimental 2^- band, starting at $E_x = 4.97$ MeV in ^{20}Ne. The states of this band have a dominant $\alpha+^{16}\text{O}(3^-)$ structure [2] and, consequently, are located too high in the GCM spectrum. It is therefore more realistic to compare their energies with respect to the $\alpha+^{16}\text{O}(3^-)$ threshold, overestimated in the GCM (16.15 MeV in place of 6.13 MeV experimentally). In this way, we obtain 2^-, 3^-, 4^-, 5^-, 6^-, and 7^- resonances located at -2.56, -3.19, -2.10, -0.26, 1.77, and 4.95 MeV with respect to the $\alpha+^{16}\text{O}(3^-)$ threshold. The corresponding experimental values are -5.90, -5.24, -3.86, -2.41, -0.25, and 2.48 MeV, respectively [15]. The theoretical $E2$ transition probabilities are 29.3, 35.5, and 58.5 $e^2\,\text{fm}^4$ for the $4^- \rightarrow 2^-$, $5^- \rightarrow 3^-$, and $6^- \rightarrow 4^-$ transitions, whereas the experimental counterparts are 3.2, 87 $\pm$ 19, and 55 $\pm$ 19 e^2 fm^4 respectively.

The multicluster approach was partly motivated by an investigation of the 0_2^+ and 0_3^+ bands in ^{20}Ne; the 0^+ and 2^+ members of these bands [$E_x(0_2^+) = 6.73$ MeV, $E_x(0_3^+) = 7.19$ MeV, $E_x(2_2^+) = 7.42$ MeV, and $E_x(2_3^+) = 7.83$ MeV] strongly affect the $^{16}\text{O}(\alpha,\gamma)^{20}$Ne capture cross section in the energy range covered by experiments [19]. These bands have been described by Fujiwara *et al.* [20] in the orthogonality condition model (OCM) involving $\alpha+^{16}$O and $^{12}\text{C}+^{8}$Be configurations. The OCM includes antisymmetrization effects but its application requires some parameters which are difficult to evaluate. The present five-α GCM approach does not reproduce the 0_2^+ and 0_3^+ bands. We have performed a few simplified calculations (i.e., with a single generator coordinate R between α and ^{16}O) with different ^{16}O configurations. However, none of these investigations gives any evidence for excited 0_2^+ or 0_3^+ bands. Two reasons can be considered: (i) the states of these bands present a dominant $^{12}\text{C}+^{8}$Be structure and therefore require an explicit treatment of this channel; (ii) their S=1 component, which is missing in an α model, might be important. The inclusion of the $^{12}\text{C}+^{8}$Be channel in the present basis does not raise any theoretical problem, but the projection over good quantum numbers of ^{12}C and ^{8}Be would require 11-dimensional integrals for the GCM matrix elements! An S=1 component might be taken into account through $^{19}\text{F}+p$ and $^{19}\text{Ne}+n$ configurations for example, but this extension is far beyond the α model.

V. $\alpha+^{16}$O ELASTIC PHASE SHIFTS AND THE $^{16}\text{O}(\alpha,\gamma)^{20}$NE CROSS SECTION

Elastic phase shifts are presented in Fig. 4 for the different models; the Majorana parameters are identical to those of Sec. IV. The general shape of the phase shifts does not change significantly from one description to another. However, as we pointed out in Sec. IV A, Pauli resonances appear beyond 10 MeV and introduce changes of 180° in the phase shifts. In the α model, the broad resonances of the 0_4^+ band have slightly larger energies than in the $\alpha+^{16}$O two-center model. The sensitivity to excited channels has been shown in $\alpha+^{12}$C scattering [5] to decrease when the ^{12}C binding energy reaches its maximum with respect to R_C. This saturation effect is confirmed in the present $\alpha+^{16}$O investigation, where the role of the $\alpha+^{16}\text{O}(3^-, 1^-)$ excited channels is rather small. In negative parity, the differences between the phase shifts are mainly around the resonances, whose energies slightly differ in the three models.

The $^{16}\text{O}(\alpha,\gamma)^{20}$Ne S-factors are presented in Fig. 5, where we display the contributions of the initial partial waves $\ell = 0$ and 2. They are computed in the MRM framework, from matrix elements of the $E2$ operator between $\alpha+^{16}$O scattering states and ^{20}Ne bound-state wave functions. The $\ell = 0$ transitions are enhanced by

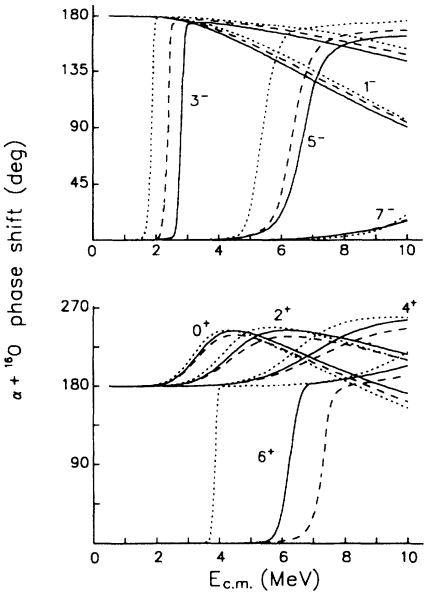

FIG. 4. α+^{16}O elastic phase shifts. The dotted, dashed, and solid lines correspond to the two-center and five-center $\alpha + ^{16}\mathrm{O}(0^+)$, and five-center $\alpha + ^{16}\mathrm{O}(0^+, 3^-, 1^-)$ models respectively.

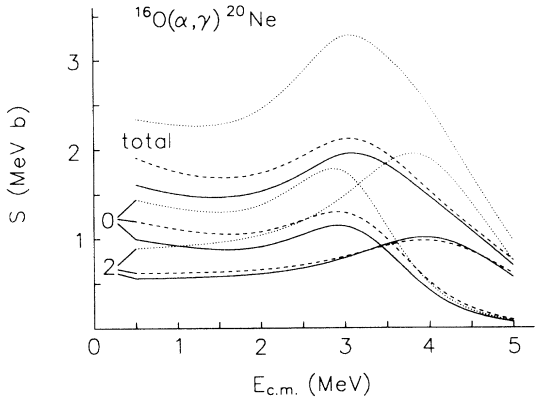

FIG. 5. $^{16}\mathrm{O}(\alpha,\gamma)^{20}\mathrm{Ne}$ S-factors, with the $\ell = 0$ and $\ell = 2$ contributions. The dotted, dashed, and solid lines correspond to the two-center and five-center $\alpha + ^{16}\mathrm{O}(0^+)$, and five-center $\alpha + ^{16}\mathrm{O}(0^+, 3^-, 1^-)$ models, respectively.

Coulomb effects, whereas the $\ell = 2$ component is favored by larger photon energies for transitions to the ground state. Let us recall that, at the long wavelength approximation, $E1$ transitions between $T = 0$ states are forbidden, and odd ℓ values are therefore missing in the total cross section. The energy dependences are similar in the different approaches. The slope of the $\ell = 0$ S factor at zero energy is mainly given [21] by the binding energy of the final state and by the scattering length a, for which we have $a = -3.10 \times 10^6$ fm, -2.45×10^6 fm, and -2.45×10^6 fm in the two-center, five-center (0^+), and five-center $(0^+, 1^-, 3^-)$ models respectively. On the contrary, the amplitude of the S-factor is more dependent on the ^{16}O description.

VI. CONCLUSION

This work aims at investigating an extension of the α model to α+^{16}O scattering, where ^{16}O wave functions are described by a four-α tetrahedral structure. This procedure significantly improves the ^{16}O description with respect to the one-center shell model. The multicluster model requires the calculation of 7 dimensional integrals for the GCM matrix elements, but this problem can be overcome with the current computer facilities and with an efficient vectorization of the codes.

In addition to the improvement of the ^{16}O binding energy, a multicluster description allows a straightforward inclusion of some excited states. At low energies, the present study shows that distortion effects, due to excited channels, are small provided that the $^{16}\mathrm{O}(0^+)$ binding energy is minimum. However, the role of excited configurations might be underestimated here because of the too-high theoretical thresholds. In addition, it might be more important in other systems, where a similar multicluster model can be applied. The need for accurate low-energy cross sections in astrophysical applications deserves an extension of the model to other systems, involving a $0s$ particle and a four-center nucleus described by α and $0s$ clusters. However, in order to keep realistic computer times, the tetrahedral nucleus should contain an equilateral structure of three α particles. The symmetry of this configuration is currently important for the feasibility of multicluster studies. This model might be applied to reactions such as $^{13}\mathrm{N}(\mathrm{p},\gamma)^{14}\mathrm{O}$ or $^{15}\mathrm{O}(\alpha,\gamma)^{19}\mathrm{Ne}$ for example.

ACKNOWLEDGMENTS

We thank the Services de Programmation de la Politique Scientifique for a supercomputer grant on the CRAY-YMP computer of the ULB-VUB. This work presents research results of the Belgian program on interuniversity attraction poles initiated by the Belgian Prime Minister's Office of Science Policy Programming. The scientific responsibility is assumed by its authors. One of us (P.D.) is chercheur qualifié FNRS.

[1] D. Brink, in *Nuclear Structure and Nuclear Reactions*, Proceedings of the International School "Enrico Fermi," Course XXXVI, Varenna, 1965, edited by M. Jean and R.A. Ricci (Academic, New York, 1966), p. 247.

[2] Y. Fujiwara, H. Horiuchi, K. Ikeda, M. Kamimura, K. Katō, Y. Suzuki, and E. Uegaki, Prog. Theor. Phys. Suppl. **68**, 29 (1980).

[3] H. Horiuchi, K. Ikeda, and Y. Suzuki, Progr. Theor.

Phys. Suppl. **52**, 89 (1972); A.C. Merchant and W.D.M. Rae, Nucl. Phys. **A549**, 431 (1992).
[4] P. Descouvemont and D. Baye, Phys. Rev. C **36**, 54 (1987).
[5] P. Descouvemont, Phys. Rev. C **44**, 306 (1991); **47**, 210 (1993).
[6] P. Descouvemont and D. Baye, Phys. Lett. **127B**, 286 (1983).
[7] C. Rolfs and W.S. Rodney, *Cauldrons in the Cosmos* (The University of Chicago, Chicago, 1988), p. 384.
[8] K. Wildermuth and Y.C. Tang, *A Unified Theory of the Nucleus* (Vieweg, Braunschweig, 1977), p. 41.
[9] Y.C. Tang, in *Topics in Nuclear Physics II*, edited by T.T.S. Kus and S.S.M. Wong, Lecture Notes in Physics, Vol. 45 (Springer, Berlin, 1981), p. 572.
[10] D. Baye and P. Descouvemont, in *Proceedings of the Sapporo International Symposium on Developments of Nuclear Cluster Dynamics*, Sapporo, Japan, 1988, edited by Y. Akaishi *et al.* (World Scientific, Singapore, 1989), p. 6.
[11] D. Baye, P.-H. Heenen, and M. Libert-Heinemann, Nucl. Phys. **A291**, 230 (1977).
[12] D. Baye and P. Descouvemont, Nucl. Phys. **A407**, 77 (1983).
[13] A.B. Volkov, Nucl. Phys. **74**, 33 (1965).
[14] D.R. Tilley, H.R. Weller, and C.M. Cheves, Nucl. Phys. **A564**, 1 (1993).
[15] F. Ajzenberg-Selove, Nucl. Phys. **A475**, 1 (1987).
[16] C.W. de Jager, H. de Vries, and C. de Vries, Atomic Nucl. Data Tables **14**, 479 (1974).
[17] H. Walliser, H. Kanada, and Y.C. Tang, Nucl. Phys. **A419**, 133 (1984).
[18] M. Kruglanski and D. Baye, Nucl. Phys. **A548**, 39 (1992).
[19] K.H. Hahn, K.H. Chang, T.R. Donoghue, and B W. Filippone, Phys. Rev. C **36**, 892 (1987); H. Knee *et al.*, *Annual Report of the Institut für Strahlenphysik* (Stuttgart University, Stuttgart, 1991), p. 31.
[20] Y. Fujiwara, H. Horiuchi, and R. Tamagaki, Prog. Theor. Phys. **61**, 1629 (1979).
[21] D. Baye and P. Descouvemont, Ann. Phys. **165**, 115 (1985).